Mesoscopic hierarchic polarization structure in the relaxor ferroelectrics Pb[(Mg_{1/3}Nb_{2/3})_{1-x}Ti_{x}]O_{3}

K. Namikawa, M. Ishino, M. Matsushita, K. Ohwada, M. Kishimoto, J. Mizuki, N. Hasegawa, and M. Nishikino

Phys. Rev. B **100**, 184110 — Published 14 November 2019

DOI: 10.1103/PhysRevB.100.184110

Mesoscopic hierarchic polarization structure in relaxor ferroelectrics $Pb[(Mg_{1/3}Nb_{2/3})_{1-x}Ti_x]O_3$

K. Namikawa[1]*, M. Ishino [2], M. Matsushita[3]**, K. Ohwada[4, 5], M. Kishimoto[2], J. Mizuki[5], N. Hasegawa[2], and M. Nishikino[2]

[1]*Department of Physics, Tokyo Gakugei University, 4-1-1 Nukuikitamachi, Koganei-shi, Tokyo 184–8501, Japan*

[2]*Quantum Beam Science Research Directorate, National Institutes for Quantum and Radiological Science and Technology, 8–1–7 Umemidai, Kizugawa-shi, Kyoto 619–0215, Japan*

[3]*Research Laboratories, JFE Mineral Co., Ltd., 1 Niihama, Chuou, Chiba-shi, Chiba 260–0826, Japan*

[4] *Quantum Beam Science Research Directorate, National Institutes for Quantum and Radiological Science and Technology, 1–1–1 Kouto, Sayo, Sayo-gun, Hyogo 679–5148, Japan*

[5]*Graduate School of Science and Technology, Kwansei Gakuin University, 2-1 Gakuen, Sanda-shi, Hyogo 669–1337, Japan*

* Corresponding author, electric mail: namikawa@u-gakugei.ac.jp

** Retired from *Research Laboratories, JFE Mineral Co., Ltd.*

Mesoscopic polarization structures such as polar nanoregions and polarization domain walls are the key factors that connecting microscopic fundamental polarization structures with macroscopic practical dielectric properties. Snapshot observation of domain in the relaxor-ferroelectrics $Pb[(Mg_{1/3}Nb_{2/3})_{1-x}\ Ti_x]\ O_3$ just vicinity of morphotropic phase boundary region was performed by use of 7 ps single shot soft X-ray laser pulse. A self-assembled evolution of oblique polarization domain was observed in $Pb[(Mg_{1/3}Nb_{2/3})_{72.2}\ Ti_{27.8}]\ O_3$ under the sample temperature decreased with thermal equilibrium condition. Based on energetic discussion, anti-phase shift of

domain wall pairs keeping with flat boundaries was proposed for the dielectric response. A sharp enhancement in dielectric response at the vicinity of morphotropic phase boundary region reported previously was recognized as an evidence for hierarchic nature of the present oblique polarization domain wall.

PACS numbers: 77.80. Jk,77.80. Dj,78.70. Ck, 78.47.D-

Relaxor-ferroelectrics has been interested in their large dielectric response and utilized for many dielectric devices. Meanwhile, advantageous properties of $Pb[(Mg_{1/3}Nb_{2/3})_{1-x}Ti_x]O_3$ (PMN–x%PT), which is an isomorphous solid solution between $Pb(Mg_{1/3}Nb_{2/3})O_3$ and $PbTiO_3$, is one of the most popular material that attracted interests not only in industrial applications[1,2] but also, in fundamental condensed matter physics.[3-5] It is well known that some macroscopic properties of solid can never be resolved simply into microscopic nature of crystal structure and electronic states but originate inherently in the mesoscopic level hierarchy.[6,7] Mesoscopic polarization structures such as polar nanoregions (PNRs)[8] and polarization domain walls[9] are certainly the matter of this kind that connecting microscopic fundamental polarization structures with macroscopic practical dielectric properties.

The structural symmetry of PMN–x%PTs in the paraelectric phase is cubic; however structural

symmetry in the ferroelectric phase varies depending on PT concentration.[10] The structural symmetry in the ferroelectric phase around room temperature changes from rhombohedral to monoclinic and finally changes to tetragonal as the PT concentration increasing.[1] The morphotropic phase boundary (MPB) region appears between 31%PT concentration and 37%PT concentration.[11-14]

It was reported that PNRs appear in PMN-x%PT below 30%PT and increase the size as the concentration of PT increases. Matsuura et al. investigated the sizes of PNRs in PMN–x%PT samples between 0%PT and 40%PT using diffuse neutron scattering measurement.[15] Close to room temperature, the sizes were estimated to be 1.3 nm, 3.4 nm, and 35 nm for 0%PT, 10%PT, and 20%PT samples, respectively. There was no diffuse scattering for PMN–30%PT and PMN–40%PT samples. Guo et.al, using diffuse x-ray scattering measurement,[16] observed 10 nm × 17nm PNRs aligned periodically at 28%PT sample under dc field when the sample is near the phase transition temperature. The disappearance of the diffuse scattering indicates the appearance of long-range ferroelectric order, which is associated with macroscopic polarization domains. Bai et. al. observed spindle like macrodomains ~1 μm in width and ~40 μm in length in PMN–30%PT samples at room temperature by polarized optical microscopy.[17]

The origin of a large dielectric response for PMN−x%PT observed in the MPB region has been assigned to the polarization rotation, which is thought to be related to the polarization direction easy to rotate in monoclinic phase.[18] While, Matsushita *et al*. observed a sudden sharp enhancement of the

dielectric response ε_r from ~4,500 up to ~7,500 around 28% PT concentration, however the origin of this anomalous dielectric response is yet to be resolved.[19] We show dielectric constants for PMN–x%PT as a function of PT concentration in Fig. 1, which is reconstructed from Fig. 7 in Ref. 19. The dielectric constants increase suddenly at the region around 28%PT concentration which is situated just below the MPB region indicated by the meshed area in the figure. The lower vicinity of MPB region, where the PT concentration ranges from 28% to 30%, is a singular region at this region PNRs disappear and polarization domains appear. Sudden increase in dielectric constants at this region could not be explained by the polarization rotation model as applied to monoclinic phase because the crystal symmetry at this region is the rhombohedral. We need another mechanism which is based inherently on the mesoscopic nature of the polarization structure.

Shimizu *et.al*. investigated the correlation length of Bragg reflection by use of Ti-composition-gradient crystal.[20] Negative correlation between electric response and domain size was found in this region. However, the distribution of the residual strain is by no means homogeneous in the Ti-composition-gradient crystal. Residual strain caused by the cooling process suffers the growth of the domain size in crystal. Direct observation of mesoscopic polarization structure by use of single-composition crystals is highly expected to clarify the nature of above-mentioned sudden enhancement of the dielectric response around 28%PT.

Yan *et.al*. pointed out the dielectric permittivity of PMN-33%PT strongly depend on the

cooling rate across the relaxor-ferroelectric phase transition temperature.[21] Okino *et.al*. confirmed the cooling rate dependences of the dielectric constant and observed the cooling rate dependence of grain size.[22] Viehland *et*. *al*. pointed out that motion of domain boundary contributes to the dielectric response.[23] Gorfman *et*. *al*. investigated the nanoscale changes in ferroelectric domain walls by observation of temperature correlation of X-ray speckle patterns.[24] Evolution of the mesoscopic secondary polarization structures of PMN–x%PT around 28%PT in cooling has a crucial importance for understanding the hierarchic nature of the relevant anomalous dielectric properties.

We investigate temperature evolution of domain structures at just below the MPB region under two different cooling rates; thermal equilibrium condition and non-equilibrium condition. The soft X-ray (SXR) pulse laser with a wavelength of 13.9 nm and a pulse width of 7 ps is a suitable tool for investigating the polarization domains through the birefringence.[25] We investigate the evolution of the mesoscopic secondary polarization structures of PMN–x%PTs by use of the picosecond speckle technique of SXR pulse laser. After the discussion of dynamics of domain wall fluctuation, we show an illustration of response of the mesoscopic polarization structure to the external electric field which is responsible for the anomalous dielectric constants.

PMN−x%PT samples with 26.6%PT, 27.8%PT, and 28.3%PT were grown in the [110] direction using the one batch melts Bridgeman method by spontaneous nucleation. These values of PT concentration have ambiguity less than 0.6%. Details of the crystal growth have been previously

described by one of the present authors and his collaborators.[19] The temperature T_m at which the dielectric constant of the sample attained its maximum (measured by an external field of 1 kHz) was 412 K for PMN–26.6% PT, 418 K for PMN–27.8% PT, and 421 K for PMN–28.3% PT. The structural symmetry of the PMN–26.6%PT sample crystal only transformed from cubic to rhombohedral at T_C. The structural symmetry of the PMN–27.8%PT sample crystal and PMN–28.3%PT sample crystal varied from cubic to tetragonal at the structural phase transition temperature T_C, and the tetragonal symmetry transformed again to rhombohedral at the secondary transition temperature T_{rt}. The size of the (001) slab-cut samples was $5 \times 3 \times 0.5$–0.7 mm^3. The surfaces of the samples were polished to an optical grade.

We investigated the appearance and growth of polarization domains by speckle measurements using coherent SXRs with instrumentations illustrated in Fig. 2. The SXR laser beam developed at the National Institutes for Quantum and Radiological Science and Technology (QST) have a wavelength of 13.9 nm with a bandwidth of approximately 10^{-4}, a pulse width of 7 ps, and more than 10^8 spatially coherent photons per pulse[26, 27] The SXR laser beam is a suitable tool for investigating the fluctuation of the polarization domains by use of the picosecond speckle technique through the birefringence. A vertically polarized SXR laser beam, prepared by a plane mirror with a 45° incidence angle, was focused on the sample using a spherical mirror. The diameter of the focal spot at the sample position was 100 μm. The glancing angle was 10° with respect to the sample surface.

The SXR laser beams reflected through birefringence from spatially distributed polarization domains interfered with each other and resulted in speckle patterns. The speckle patterns were recorded by a charge-coupled device (CCD) camera placed 140 mm downstream from the sample. In this experimental setup, the observable maximum domain size was approximately 415 × 73 μm^2, which was restricted by the pixel size of the CCD camera (13.5 × 13.5 μm^2) and the incident angle of the SXR laser beam. The spatial resolution of the calculated autocorrelation function in this study was approximately 300 nm, which was restricted by the adoption area of an image taken by the CCD camera.

Coherent SXR speckle patterns for PMN–26.6%PT, PMN–27.8%PT, and PMN–28.3%PT samples observed at temperatures 428K (above T_m), 398K (between T_m and T_{rt}), and 353K (below T_{rt}) during cooling are shown in Fig. 3. Direct beam patterns are shown for reference. Autocorrelation pattern at 353 K are also shown in Fig. 3 at the last column.

The speckle patterns for PMN−26.6%PT at each temperature are almost a mirror image of the direct beam and do not differ each other. While the speckle patterns for the PMN–27.8%PT sample and for the PMN–28.3%PT sample vary with temperatures, which means that polarization domains appearing in the sample change their sizes and shapes with the temperature. Autocorrelation images for the PMN–26.6%PT sample, for the PMN–27.8%PT sample, and for the PMN-28.3%PT sample at 353 *K* are shown in the last column in the Fig. 3. Autocorrelation image obtained by speckle

pattern of PMN–26.6%PT is just the image of incident beam. No polarization domains larger than 300 nm in size (this value is the lower limit of observation) have been observed in the PMN–26.6%PT sample. While, autocorrelation pattern obtained by speckle pattern of PMN-28.3%PT shows a few large domains exist. In contrast, autocorrelation pattern obtained by speckle pattern of PMN–27.8%PT revealed ordered oblique stripe domains. However, even if polar nanoregions less than 300nm exist in 26.6%PT, 27%PT, and 28%PT samples, they could not be recognized due to the limit of resolution.

Here after we concentrate the investigation on the origin and the behavior of this ordered oblique stripe domains observed at PMN–27.8%PT. The appearance of the ferroelectric phase in the PMN–27.8%PT sample was confirmed by x-ray diffraction and capacitance measurements. The temperature dependences of the lattice constants and the widths of rocking curves were measured at BL22XU in SPring-8.[28] The sample temperature decreased from 430 K to 360 K on cooling process and increased from 360 K to 430 K on heating process. No external electric field was applied while the x-ray diffraction measurements. The lattice constants and the width of the rocking curve were observed around the 200 Bragg peak position. The results are shown in Figs. 4 (a) and 4(b). Cubic to tetragonal phase transition took place at 407 K on cooling. The lattice constant, a_C, in the cubic phase split into two lattice constants, a_T and $c_{T,}$ in the tetragonal phase. We have indicated the structural transition temperatures on cooling (heating) as T_C^c (T_C^h). The expansion of the rocking

curve width took place at 2–4 K below T_C^c on cooling. The dielectric capacitance was measured by using an LCR meter. Fig. 4(c) shows the temperature and frequency dependence of capacitance. The capacitance shows a hysteresis loop upon cooling and heating. The capacitance has its maximum at T_M (= 418 K), and the capacitance also shows abrupt changes at T_C^c and T_C^h. The structural changes and the dielectric behaviors around the structural phase transition temperatures are coincide with each other.

We show two series of observed coherent SXR speckle patterns for the PMN–27.8%PT sample at four different temperatures below T_C^c in Figs. 5(a) and 5(b). Speckle patterns shown in Fig. 5(a) were observed on thermally non-equilibrium condition, while those in Fig. 5(b) were observed on thermally equilibrium condition. On cooling in thermal non-equilibrium condition, the sample temperature was decreased by 5K/2min step, and then SXR speckle patterns were observed shortly. In thermal equilibrium condition, in contrast, the sample temperature was decreased by 1K/5min step and held for about 20 minutes before SXR speckle measurements. Speckle patterns reflect the evolution of distributions of polarization domains because the origin of the soft x-ray speckles is birefringence. Information about domain sizes and adjacent domain distances can be evaluated from a spatial autocorrelation function which is calculated from the intensity distributions of the speckle patterns. Figures 5(c) and 5(d) show spatial images of autocorrelation functions derived from the speckle patterns shown in Figs. 5(a) and 5(b), respectively.

Both domain shapes in Figs. 5(c) and 5(d) gradually become distinct with decreasing the sample temperature. As shown in Figs. 5(c) and 5(d), polarization domain shapes, which appeared in the PMN–27.8%PT sample just below the phase transition temperature (403 K or 402 K), were irregular. However, with decreasing temperature, these irregularly shaped polarization domains evolved into stripe-shaped periodic domains. The domain patterns are oblique stripe-shaped periodic structures toward the [-110] direction. The domain shapes in Fig. 5(c) are irregular and domain boundaries are unclear. However, the domain shapes in Fig. 5(d) differ from those in Fig. 5(c), and domain boundaries of the stripe-shaped structures become clear and the width of each domain becomes narrower as the sample temperature decrease. The stripe-shaped oblique domains are 90° domains with polarization directions of [010] and [100], which are parallel and perpendicular to the polarization of the incident SXR laser beam, respectively. Figs. 5(e) and 5(f) are cross-section intensity profiles perpendicular to the domain walls derived from autocorrelation functions shown in Figs. 5(c) and 5(d), respectively.

Shot by shot fluctuation of the cross-section intensity profiles are illustrated in Fig. 6. In case of non-equilibrium condition, each profile in Fig. 6(a) shows a different pattern depending on the instant at the observation even short rang correlation looks similar. On the other hands, under the equilibrium condition each profile in Fig. 6(b) is surprisingly similar at any instant of the observation. Even a little fluctuation in width of the domains are identified depending on the instant of the

observation, domain boundaries look as keeping a similar shape at any instant of observation. The stripe domains look very steady.

At the temperatures range around 385 K–400 K Kutnjak *et al*. reported an appearance of excess heat capacity in a PMN–29.5%PT sample,[29] whose PT concentration was close to our PT concentration of 27.8%. The excess heat capacity means the existence of additional entropy, which can be expressed as $\Delta S = \int \left(C_{\mathrm{p}}/T\right) \mathrm{d}T$, where S, C_{p}, and T is entropy, heat capacity, and temperature, respectively. The result shown in Fig. 1a in their article means reduction in entropy took place when the crystal was cooled from 400 K to 385 K. This temperature range coincides with those at which the evolution of stripe-shaped polarization domains occurred in our experiments. The evolution of stripe-shaped domains observed in the PMN–27.8%PT sample during cooling in thermal equilibrium condition can be recognized as a self-assemble process for polarization domains accompanied by a release in entropy.

Polarization gradient in the [-110] direction within the oblique stripe-shaped 90° polarization domains was small, whereas that in the [110] direction was large at the domain wall. The growth of 90° stripe-shaped polarization domains toward the [-110] direction was a self-assemble process accompanied by anisotropies in the polarization gradients between the [-110] and [110] directions.

When the sample temperature decreases rapidly, fluctuations of polarizations are significant. These large fluctuations of polarization result in wider domains and unclear domain boundaries, as

shown in Fig. 5(c). Domain boundaries in thermal non-equilibrium condition looks disordered with indistinct and uneven boundary. On the other hand, when the sample temperature decreases in thermal equilibrium condition, fluctuations of polarizations are small, causing the presence of the stripe-shaped 90° polarization domains with narrower widths and sharp boundaries as shown in Fig. The stripe-shaped 90° polarization domain is known as elastic strain highly relaxed domain structure.5(d). Each image in Fig. 5 shows a snapshot picture of domain with fluctuating domain walls, however, in thermal equilibrium condition, the domain boundary observed by a single shot speckle are flat and smooth. Each domain boundaries looks keeping a common parallel domain wall at any instance of observation as shown in Fig. 6(b).

Chu *et al*. pointed out in their phase field simulation[9] that the compressive strain induces active fluctuation in the oblique 90° domain wall. This situation is applicable to our result. On application of external electric field to [010] direction, deformation of unit cell takes place; lattice constants in (001) plane begins to elongate to the [010] and shrink to the [100]. As the results, compressive strain takes place toward [100] within the (001) plane. The stripe-shaped domain wall becomes easy to move by an external electric field.

When an external electric field is applied to [010] direction, which is parallel to the polarization direction in one of the 90° stripe-shaped oblique domains, then the domain area relevant to the polarization direction increases. In this case, the domain wall shifts reversibly with

little increase in free energy, as pointed by Zhang and Li.[1, 30] If increase in the polarization area take place by the antiphase shift of parallel domain wall pairs as mentioned by Pertsev et al.[31] for the case of ferroelectric thin film, then the increase in the excitation energy of the polarization is suppressed because there is no need for the creation of new domain walls in this mode. A schematic drawing of this situation is shown in Fig. 7. A pair of domain walls face to anti-phase shift keeping with flat boundaries at application of electric field. In this mode, relaxation of elastic strain is almost preserved, while the electrostatic energy is reduced by $\Delta p \cdot E$. In case of indefinitely shaped polarization domains, on the contrary, if an increase in the area of the relevant polarization domains occur by the elongation of the domain wall, the cost of excitation energy for new polarization area is larger because the creation of new domain walls is required. If the shift of domain wall pairs occurs as a collective mode by an external alternative electric field, then the suppressed shift-energy of wall pairs is more decreased. Strong enhancement in dielectric coefficients in Fig. 1. can be recognized as an evidence for collective excitation of the oblique 90° domain wall pairs when an external alternative electric field applied.

Tang et. al[32] observed frequency dependent of dielectric constant between 50Hz and 10,000Hz in 26%PT crystal. No sudden enhancement in dielectric constant is identified. Stripe type domain less than 300nm like our 27.8%PT sample may not be exist even in our 26.6% PT sample.

The large dielectric responses observed in PMN–x%PTs around the PT concentration 28% can

be attributed to a characteristic nature of the self-assembled oblique 90° polarization domains to an external electric field. This peculiar response of the polarization domain walls to an external electric field is recognized as an evidence for the hierarchical characteristics of the relevant mesoscopic polarization structure. A collective mode domain wall response is anticipated in our oblique 90° polarization domain. The self-assembly of 90° polarization domains and the manifestation of mesoscopic hierarchic characteristics clarified in our study are significant for further research concerning the basic ferroelectric response and performance of relaxor-ferroelectrics.

Acknowledgments

The authors acknowledge the assistance of the QST staff, in addition to D. Shimizu and J. Sakamoto of Kwansei Gakuin University. One of the authors, M. I., thanks Y. Yonetani and M. Kono of QST for their advice regarding FFT calculations. The synchrotron radiation experiments were performed at BL22XU of Spring-8 with the approval of Japan Synchrotron Research Institute (JASRI) (Proposals No. 2012B3713). This work was supported by Grant-in-Aid for Scientific Research (16K05395). This work was supported in part by a CREST-JST program.

[1] F. Li, S. Zhang, Z. Xu, X. Wei, J. Luo, and T. R. Shrout, J. Appl. Phys. **108**, 034106 (2010).

[2] S. Zhang, and F. Li, J. Appl. Phys. **111**, 031301 (2012).

[3] D. Phelan, C. Stock, J. A. Rodriguez-Rivera, S. Chi, J. Leao, X. Long, Y. Xie, A. A. Bokov, Z.-G. Ye, P. Ganesh, and P. M. Genhring, Proc. Natl. Acad. Sci., **111,** 1754 (2014)

[4] M. E. Manly, D. L. Abernathy, R. Sahul, D. E. Parshall, J. W. Lynn, A. D. Christianson, P. J. Stonaha, E. D. Specht, and J.D. Budai, Sci. Adv. **2016;2**: e1501814 (2016).

[5] L. Shu, M. Wan, X. Jiang, F. Li, N. Zhou, W. Huang, and T. Wang, AIP Advances **7**, 015010 (2017).

[6] K. Ishida, and K. Nasu, J. Phys. Soc. Jpn. **81**, 06378 (2012).

[7] D. Fu, H. Taniguchi, M. Itoh, S. Koshihara, N. Yamamoto, and S. Mori, Phys. Rev. Lett. **103**, 207601 (2009).

[8] D. Viehland, M. –C. Kim, Z. Xu, and J. –F. Li, Appl. Phys. Lett. **67**, 2471 (1995).

[9] P. Chu, D. P. Chen, Y. L. Wang, Y. L. Xie, Z. B. Yan, J. G. Wan, J. –M. Liu, and J. Y. Li, Sci. Rep. **4**, 5007; DOI:10.1038/ srep05007 (2014).

[10] S. W. Choi, T. R. Shrout, S. J. Jang, and A. S. Bhalla, Ferroelectrics **100**, 29 (1989).

[11] O. Noblanc, P. Gaucher, and G. Calvarin, J. Appl. Phys. **79**, 4291 (1996).

[12] B. Noheda, D. E. Cox, G. Shirane, J. Gao, and Z. G. Ye, Phys. Rev. B **66**, 054104 (2002).

[13] A. K. Singh and D. Pandey, Phys. Rev. B **67**, 064102 (2003).

[14] A. K. Singh, D. Pandey, and O. Zaharko, Phys. Rev. B **74**, 024101 (2006).

[15] M. Matsuura, K. Hirota, P. M. Gehring, Z.–G. Ye, W. Chen, and G. Shirane, Phys. Rev. B **74**, 144107 (2006).

[16] Z. Guo, R. Z. Tai, H. Xu, C. Gao, G. Pan, H. Luo, and K. Namikawa, Appl. Phys. Lett. **91**, 081904 (2007).

[17] F. Bai, J. Li, and D. Viehland, J. Appl. Phys. **97**, 054103 (2005).

[18] A. K. Singh, and D. Pandey, Phys. Rev. B **67**, 064102 (2003).

[19] M. Matsushita, Y. Tachi, and Y. Iwasaki, JFE Tech. Rep. **6**, 46 (2005).

[20] D. Shimizu, S. Tsukada, M. Matsuura, J. Sakamoto, S. Kojima, K. Namikawa, J. Mizuki, and K. Ohwada, Phys. Rev. B **92**, 174121 (2015).

[21] F. Yan, P. Bao, Y. Wang, H. L. W. Chan, and C.L. Choy, Appl. Phys. Lett, **81**, 4580 (2002).

[22] H. Okino, J. Sakamoto, and T. Yamamoto, Jpn. J. Appl. Phys. **44**, 7160 (2005).

[23] D. D. Viehland, and E. H. K. Salje, Adv. in Phys. **63**, 267 (2014).

[24] S. Gorfman, A. A. Bokov, A. Davtyan, M. Reiser, Y. Xie, Z-G. Ye, A. V. Zozulya, M. Sprung, U. Pietsch, and C. Gutt, Proc. Natl. Acad. Sci. USA, 115(29), E6680 (2018).

[25] R. Z. Tai, K. Namikawa, A. Sawada, M. Kishimoto, M. Tanaka, P. Lu, K. Nagashima, H. Maruyama, and M. Ando, Phys. Rev. Lett. **93**, 087601 (2004).

[26] M. Nishikino, M. Tanaka, K. Nagashima, M. Kishimoto, M. Kado, T. Kawachi, K. Sukegawa, Y. Ochi, N. Hasegawa, and Y. Kato, Phys. Rev. A **68**, 061802(R) (2003).

[27] Y. Ochi, T. Kawachi, N. Hasegawa, M. Nishikino, T. Ohba, M. Tanaka, M. Kishimoto, T. Kaihori, K. Nagashima, and A. Sugiyama, Jpn. J. Appl. Phys. **48**, 120212 (2009).

[28] T. Shobu, K. Tozawa, H. Shiwaku, H. Konishi, T. Inami, T. Harami, and J. Mizuki, AIP Conf. Proc. 879, 902 (2007).

[29] Z. Kutnjak, J. Petzelt, and R. Blinc, Nature **441**, 956 (2006).

[30] D. Damjanovic, "Hysteresis in piezoelectric and ferroelectric materials," in *The science of Hysteresis,* edited by I. Mayergoyz and G. Bertotti (Elsevier, N. Y. 2005), Vol. 3, pp. 337-465.

[31] N, A. Pertsev and A. Yu. Emelyanov, Phys. Rev. B 65, 174115 (2002).

[32] Y. Tang, X. Wan, X. Zhao, X. Pan, D. Lin, H. Luo, J. Sun, X. Meng, and J. Zhu, J. Appl. Phys. **98**, 084104 (2005).

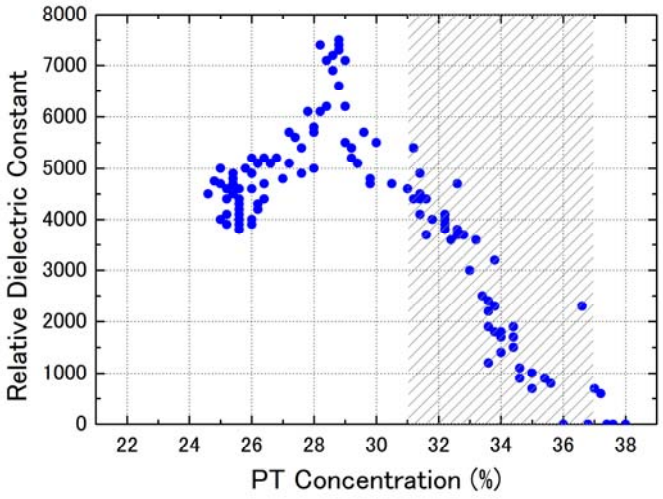

FIG. 1. PMN–x%PT dielectric constants depend on the Ti concentration. This graph was reconstructed from Fig. 7 in Ref. 19. The MPB region is indicated by the hatched area

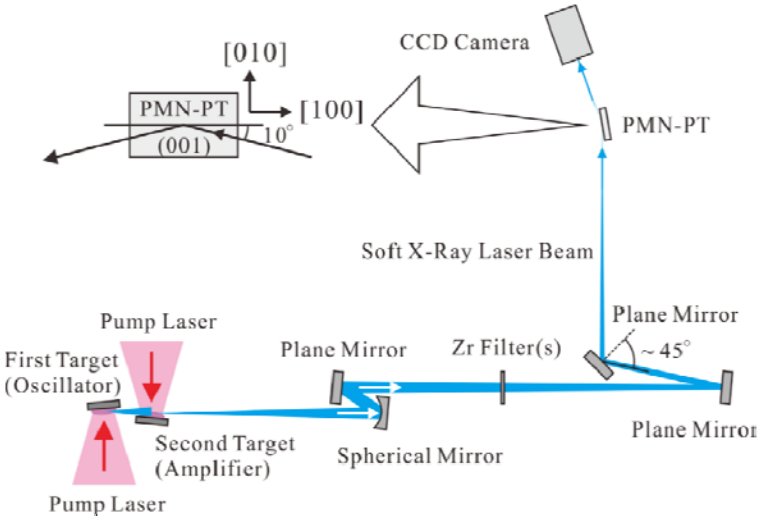

FIG. 2. Schematic of the experimental setup and temperature dependences of the coherent SXR speckle patterns. The polarized coherent SXR laser beam is focused on the sample surface, and the reflected beam from the sample is acquired by an SXR CCD camera.

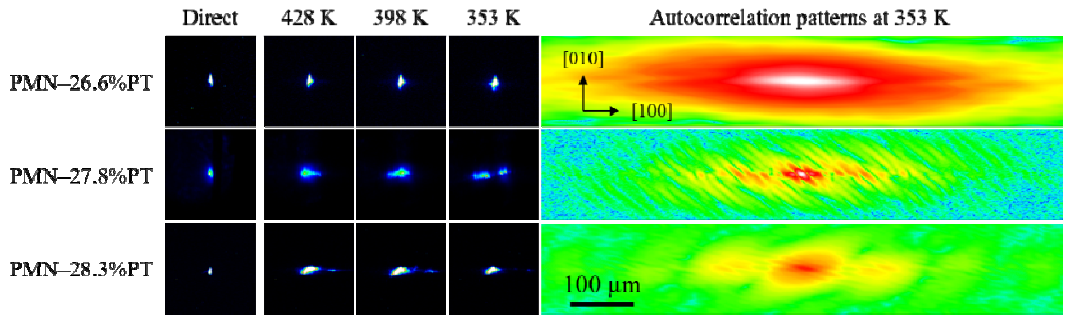

FIG. 3. Speckle patterns for PMN–26.6%PT, PMN–27.8%PT, and PMN–28.3%PT samples. Direct beam patterns are also shown for reference. Autocorrelation patterns at 353K are shown to the right side of speckle patterns.

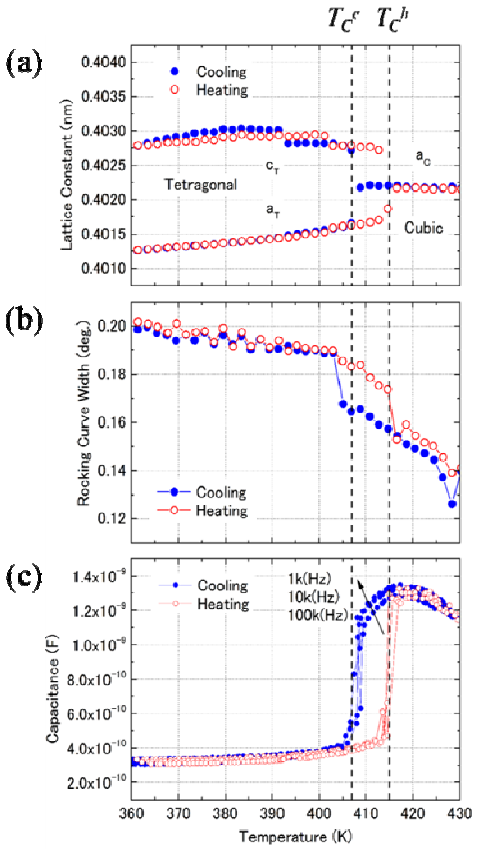

FIG. 4. Temperature dependences of (a) the lattice constant, (b) the rocking curve width (FWHM) at the 200 Bragg peak position, and (c) the capacitances for each frequency for the PMN–27.8%PT sample.

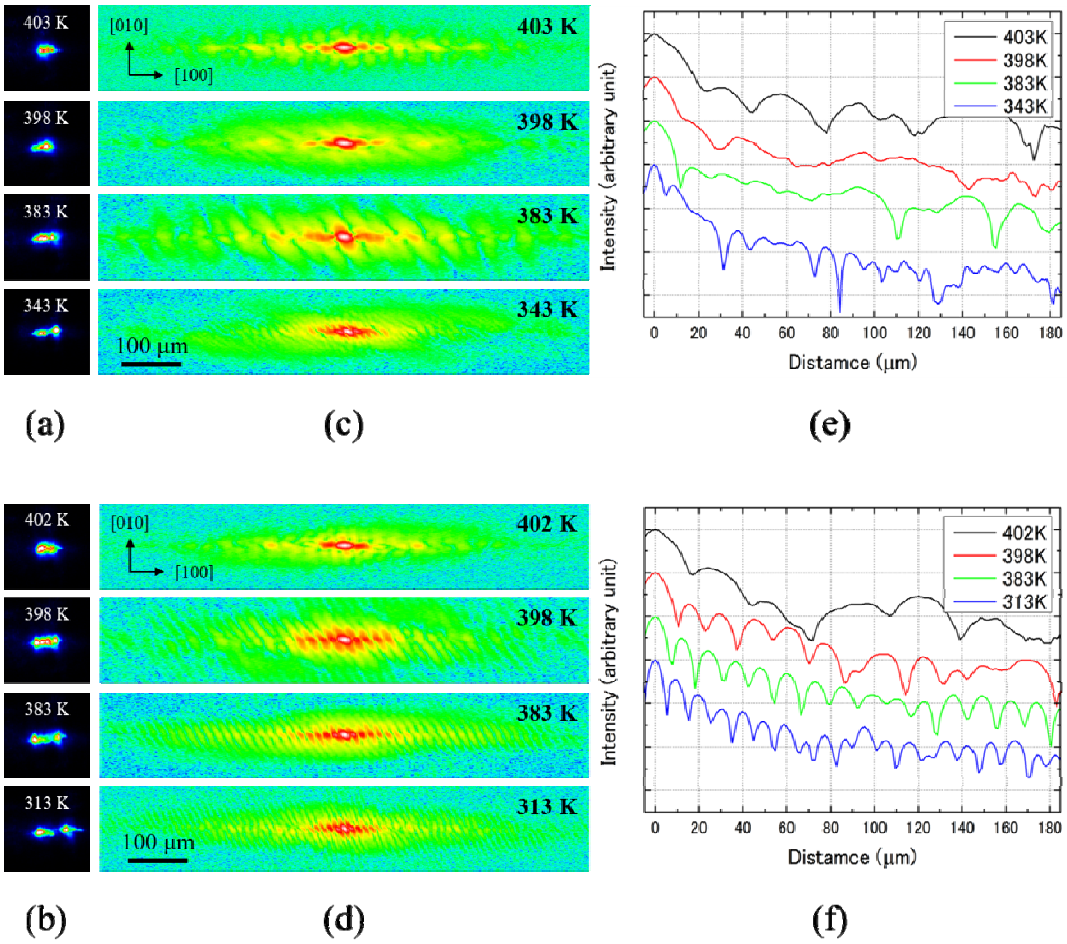

FIG. 5. Observed speckle patterns, calculated spatial correlation functions, and cross-sectional profiles of spatial autocorrelation functions. (a) and (b) Coherent SXR speckle patterns for the PMN–27.8%PT sample measured under cooling in thermal non-equilibrium and equilibrium conditions, respectively. (c) and (d) Spatial autocorrelation functions obtained from the speckle patterns shown in Figs. 5(a) and 5(b), respectively. (e) and (f) The cross-sectional profiles perpendicular to the domain walls in Figs. 5(c) and 5(d), respectively

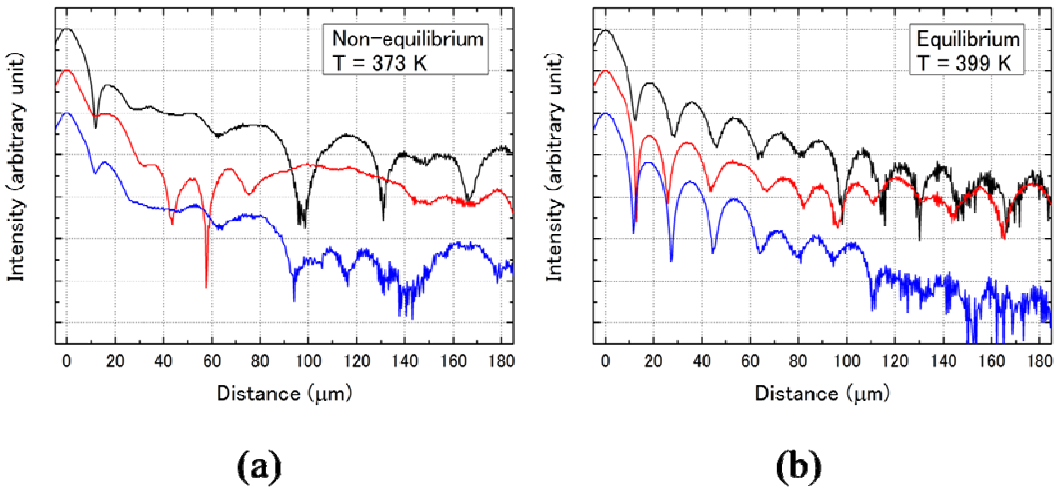

FIG. 6. Shot by shot cross-section profiles. Shot by shot fluctuation of the domain boundaries are shown. (a) Fluctuation of domain boundaries are clearly shown at non-equilibrium condition. (b) No obvious fluctuation could be recognized at equilibrium condition.

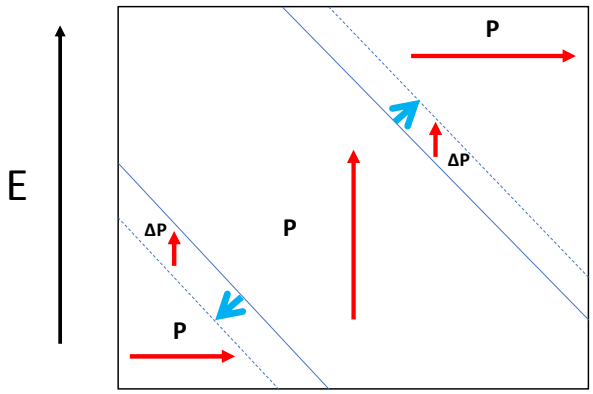

Fig. 7. Schematic model of antiphase shift of domain walls under application of electric field. Elastic strain is almost preserved at the antiphase shift of domain walls